

Indirect contributions to electron-impact ionization of Kr^{24+} , Kr^{25+} , and Xe^{43+}

M. H. Chen and K. J. Reed

High Temperature Physics Division, Lawrence Livermore National Laboratory, Livermore, California 94550

(Received 2 November 1992)

Electron-impact ionization cross sections have been calculated for Kr^{24+} and Kr^{25+} . The contributions of excitation-autoionization and resonant excitation double autoionization (REDA) were included in addition to the cross sections for direct ionization of a $3s$ electron. For Xe^{43+} the REDA contributions were extended to two times the ionization threshold. The calculations were performed using the relativistic distorted-wave and the multiconfiguration Dirac-Fock methods. For Kr^{25+} the indirect processes enhance the ionization cross section by a factor of 4. For Kr^{24+} the total cross section is about 3.5 times the direct-ionization cross section. The REDA process produces numerous strong resonances and contributes about 20% to the average ionization cross section for Kr^{24+} and Kr^{25+} and 15% to the average ionization cross section for Xe^{43+} .

PACS number(s): 34.80.Kw

I. INTRODUCTION

Electron-impact ionization is an important process in hot dense plasmas. It can affect the ionization balance, electron temperature, electron density, and level populations in the plasmas. In the past decade, theoretical and experimental studies have revealed that in many cases the contributions of indirect processes to the total ionization cross section exceeds the contribution of direct ionization [1–3]. The most important indirect process is excitation of an inner-shell electron followed by emission of an Auger electron, referred to as excitation-autoionization (EA). The EA process is routinely included in calculations of ionization cross sections. Higher-order processes such as resonant excitation followed by sequential double autoionization (REDA) [2], or by auto-double-ionization in one step [4], can also contribute to the ionization cross section. It is very difficult to include these higher-order processes because of their complexity and in most calculations they are neglected.

The effects of relativity and intermediate coupling are very significant in calculations of atomic structure and transition rates for highly charged ions [5]. Also the effects of radiative decay increase, and the effects of channel coupling diminish with increasing atomic number [6]. Hence the relativistic distorted-wave approximation and the multiconfiguration Dirac-Fock (MCDF) method are suitable for studies of electron collisions with highly charged ions.

In a series of papers we have reported studies of electron-impact ionization of Li-like ions with $Z \leq 54$ [7,8] and Na-like ions with $26 \leq Z \leq 92$ [9,10]. For Na-like ions, the REDA cross sections were included completely for Fe^{15+} [9] and partially for Xe^{43+} [10]. In these studies the EA process was found to enhance the ionization cross sections by about a factor of 4 for sodiumlike ions and by (5–10)% for lithiumlike ions. The REDA process produces many strong resonances and contributes about 30% to the average ionization cross section for Fe^{15+} [9]. In this paper we report calculations

of electron-impact ionization cross sections for Mg-like Kr and Na-like Kr including contributions from the direct, EA, and REDA processes. Our work is the first study to include the REDA process for a highly charged Mg-like ion. In addition we have extended our earlier REDA calculations for Xe^{43+} [10] to energies up to two times the ionization threshold.

II. THEORETICAL METHOD

Our calculational procedure has been described in detail in Refs. [9] and [10]. Here we outline the essential points. We performed separate fully relativistic calculations for the direct ionization cross sections, the cross sections for excitation to the intermediate autoionizing states, the energy-averaged cross sections for capture into double Auger states and the radiative and Auger transition rates.

For ionization of a $3s$ electron in a Mg-like ion, the direct, EA, and REDA processes can be described schematically by

$$e + 1s^2 2l^8 3s^2 \rightarrow 1s^2 2l^8 3s + e + e, \quad (1)$$

$$e + 1s^2 2l^8 3s^2 \rightarrow 1s^2 2l^7 3s^2 nl + e \\ \rightarrow 1s^2 2s^2 2p^6 n'l' + e + e, \quad (2)$$

$$e + 1s^2 2l^8 3s^2 \rightarrow 1s^2 2l^7 3s^2 nln'l' \\ \rightarrow 1s^2 2l^7 3s^2 n''l'' + e \\ \rightarrow 1s^2 2s^2 2p^6 nl + e + e. \quad (3)$$

Similar expressions have been given for Na-like ions in Refs. [9] and [10]. Assuming that the direct- and indirect-ionization processes are independent, the total ionization cross section σ_t is given by

$$\sigma_t = \sigma_d + \sum_i \sigma_i^{\text{ex}} B_i^{\text{A}} + \sum_k \bar{\sigma}_k^{\text{cap}} B_k^{\text{DA}}. \quad (4)$$

Here, σ_d is the direct-ionization cross section; σ_i^{ex} and $\bar{\sigma}_k^{\text{cap}}$ are excitation and energy-averaged dielectronic cap-

ture cross sections, respectively; and B_i^A and B_k^{DA} are the branching ratios for the single and sequential double Auger emission, respectively.

The single and double Auger branching ratios can be written as

$$B_i^A = \frac{\sum_j A_{ij}^a}{\sum_m A_{im}^a + \sum_k A_{ik}^r}, \quad (5)$$

and

$$B_k^{DA} = \frac{\sum_{k'} A_{kk'}^a \sum_f A_{k'f}^a}{(\sum_m A_{km}^a + \sum_n A_{kn}^r)(\sum_m A_{k'm}^a + \sum_n A_{k'n}^r)}, \quad (6)$$

where A_{ij}^a and A_{ik}^r are the Auger and radiative-transition rates, respectively.

The energy-averaged capture cross section from the initial state i to the intermediate state k in cm^2 is obtained from the inverse Auger process by detail balance [2],

$$\bar{\sigma}_k^{\text{cap}} = \frac{4.95 \times 10^{-30}}{\Delta E E_k} \frac{g_k}{2g_i} A_{ki}^a. \quad (7)$$

Here ΔE and E_k are the energy bin and Auger energy in eV; g_k and g_i are the statistical weights and the Auger rate is in units of sec^{-1} .

The direct-ionization cross sections [Eq. (1)] were calculated using a full partial-wave-expansion method [11] in which the wave functions of the bound, incident, scattered, and ejected electron wave functions were computed in Dirac-Fock-Slater potentials. Exchange was included by using completely antisymmetric final-state wave functions in the ionization amplitude. A relativistic distorted-wave method [12] was used with relativistic configuration-interaction (CI) target wave functions to calculate the cross sections for exciting the $2s$ and $2p$ electrons to the $n=3$ subshells. The CI wave functions for Kr^{25+} include states from the $2s^2 2p^6 3l$, $2s^2 2p^5 3l 3l'$, and $2s^1 2p^6 3l 3l'$ configurations. For Kr^{24+} , states from the $2s^2 2p^6 3s^2$, $2s^2 2p^5 3s^2 3l$, and $2s 2p^6 3s^2 3l$ configurations are included. The capture cross sections [Eq. (7)], and the single Auger [Eq. (5)] and double Auger [Eq. (6)] branching ratios, were computed using the detailed Auger and radiative rates. These transition rates were evaluated using the MCDF model [13,14] in intermediate coupling with configuration interaction from the same complex.

In calculating the REDA cross sections, we included the resonant states $2s^2 2p^5 3s 4l n l'$ ($n=4-7, l \leq 4$), $2s^2 2p^5 3s 3l n l'$ ($n=7-12, l' \leq 3$), $2s 2p^6 3s 3l n l'$ ($n=6-12, l' \leq 3$), $2s 2p^6 3s 4l n l'$ ($n=4-7, l' \leq 3$), and $2s^2 2p^5 3s 5l 5l'$ for Kr^{25+} and Xe^{43+} . For Kr^{24+} , similar intermediate states were included except for the last one. Extrapolation to $n=30$ was performed for the first four cases using the n^{-3} scaling for the Auger transitions. In calculations of branching ratios, all possible Auger pathways and electric-dipole radiative decays with change of principal quantum number ($\Delta n > 0$) were taken into account.

III. RESULTS AND DISCUSSION

In Tables I and II we list the ten largest excitation-autoionization cross sections calculated at approximately

TABLE I. Ten largest excitation-autoionization cross sections for Kr^{24+} at 2020 eV incident electron energy.

Level	Energy (eV)	Configuration	B^A	σ (10^{-21} cm^2)
7	1694	$(2p_{3/2} 3p_{3/2})_0$	0.990	3.89
11	1739	$(2p_{1/2} 3p_{1/2})_0$	0.997	9.85
13	1754	$(2p_{3/2} 3d_{3/2})_1$	0.763	1.19
14	1757	$(2p_{3/2} 3d_{3/2})_3$	0.862	1.17
15	1758	$(2p_{3/2} 3d_{5/2})_4$	0.764	1.44
16	1758	$(2p_{3/2} 3d_{5/2})_2$	0.771	1.35
19	1774	$(2p_{3/2} 3d_{5/2})_1$	0.203	3.56
23	1823	$(2p_{1/2} 3d_{3/2})_1$	0.187	3.58
30	2004	$(2s 3d_{5/2})_3$	1.000	1.35
31	2011	$(2s 3d_{5/2})_2$	1.000	4.06

TABLE II. Ten largest excitation-autoionization cross sections for Kr^{25+} at 2040 eV incident electron energy.

Level	Energy (eV)	Configuration	B^A	σ (10^{-21} cm^2)
18	1718	$(2p_{3/2} 3s 3p_{3/2})_{1/2}$	0.990	3.06
28	1753	$(2p_{1/2} 3s 3p_{3/2})_{1/2}$	0.973	5.75
37	1769	$(2p_{1/2} 3s 3p_{3/2})_{1/2}$	0.989	4.30
38	1770	$(2p_{3/2} 3s 3d_{5/2})_{9/2}$	1.000	0.99
47	1780	$(2p_{3/2} 3s 3d_{3/2})_{1/2}$	0.803	1.38
49	1785	$(2p_{3/2} 3s 3d_{5/2})_{3/2}$	0.714	3.77
53	1796	$(2p_{3/2} 3s 3d_{5/2})_{3/2}$	0.219	1.18
82	1834	$(2p_{1/2} 3s 3d_{3/2})_{3/2}$	0.474	3.50
101	1850	$(2p_{1/2} 3s 3d_{3/2})_{3/2}$	0.537	2.54
113	1880	$(2s 3s^2)_{1/2}$	0.989	2.41

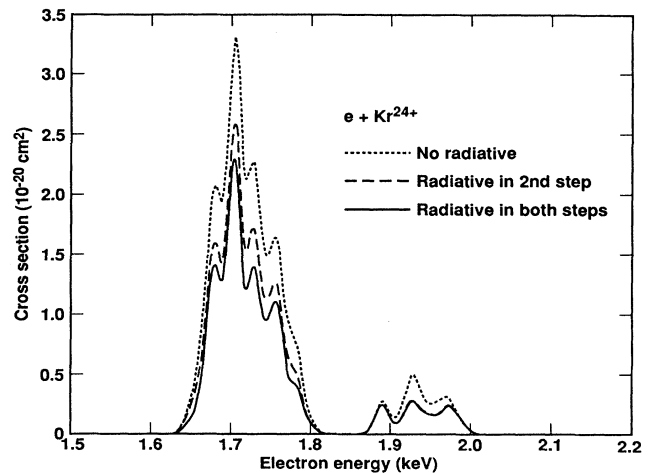


FIG. 1. REDA cross sections for the $2p^5 3s^2 4l 4l'$ intermediate states of Kr^{24+} as functions of electron energy. The dotted curve indicates the results without radiative damping. The dashed curve displays the values with radiative decay in the second step. The solid curve shows the results with radiative decay in both steps.

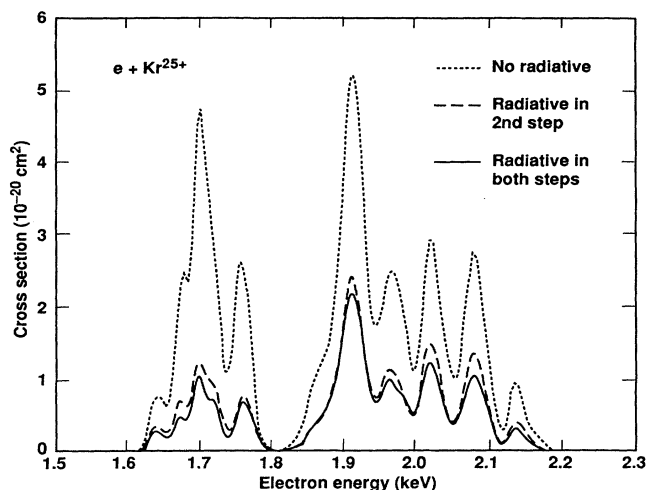


FIG. 2. REDA cross sections for the $2p^5 3s 4nl'$ intermediate states of Kr^{25+} as functions of electron energy. The symbols are the same as in Fig. 1.

twice the ionization thresholds of Kr^{24+} and Kr^{25+} , respectively. The excitation energies and branching ratios are also included in these tables. The atomic states are identified by their dominant components in the j - j coupled basis set. The notation $(2p_{3/2} 3p_{3/2})_0$ for Kr^{24+} indicates a hole in the $2p_{3/2}$ subshell and an electron in the $3p_{3/2}$ subshell coupled to give a state with total angular momentum $J=0$. The $3s^2$ closed shell is omitted in the description. For Kr^{25+} the notation $(2p_{3/2} 3s 3p_{3/2})_{1/2}$ represents a state with a hole in the $2p_{3/2}$ shell and one electron in the $3s$ and the other in the $3p_{3/2}$ subshells. The hole and electron couple to yield a total angular momentum $J=\frac{1}{2}$. These ten largest cross sections together contribute about 70% of the total EA cross sections.

The effect of radiative decay is taken into account by multiplying each excitation cross section by the appropri-

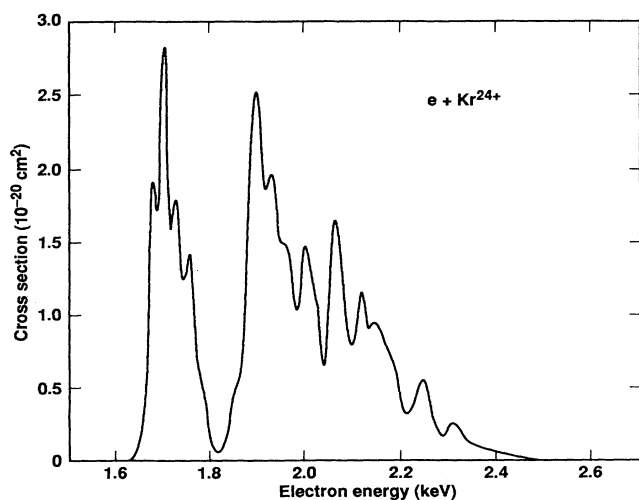


FIG. 3. Total REDA cross sections for Kr^{24+} .

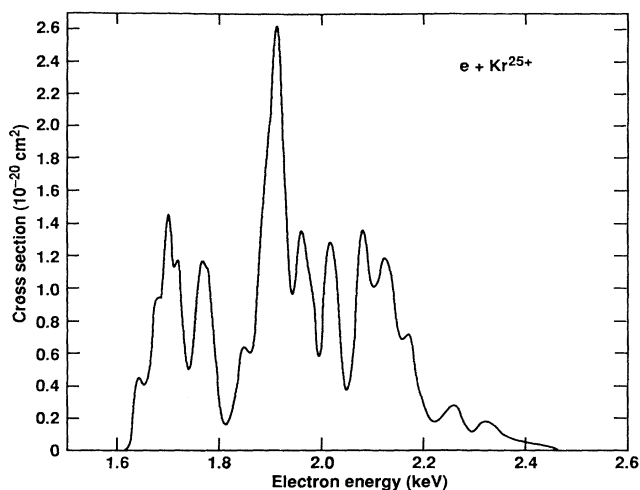


FIG. 4. Total REDA cross sections for Kr^{25+} .

ate branching ratio. Radiative decay reduces the total EA cross sections for Kr^{25+} by a factor of 2. The effect of radiative decay on the REDA cross sections of Kr^{24+} and Kr^{25+} are shown in Figs. 1 and 2, respectively. In the first step of the REDA process radiative damping produces only a 10% reduction in the cross section. There are many possible Auger-decay channels which result in a large Auger width. Consequently it is very important to include all possible Auger channels in the first step. In the second step of the REDA process radiative decay becomes more important. The REDA cross sections for Kr^{25+} and Kr^{24+} are reduced by a factor of 4 and 30%, respectively, by radiative damping in the second step. The presence of two $3s$ electrons in the Mg-

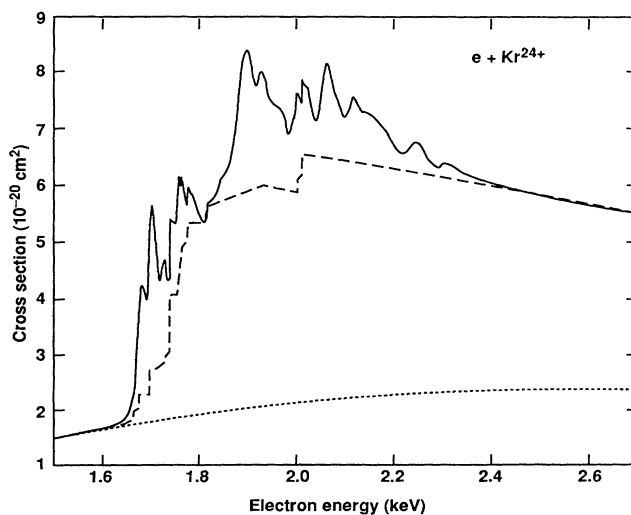


FIG. 5. Electron-impact ionization cross sections for Kr^{24+} as functions of electron energy. The dotted curve indicates the direct-ionization cross sections. The dashed curve illustrates the cross section including direct and excitation-autoionization. The solid curve represents the total ionization cross sections including the direct, excitation-autoionization, and REDA processes.

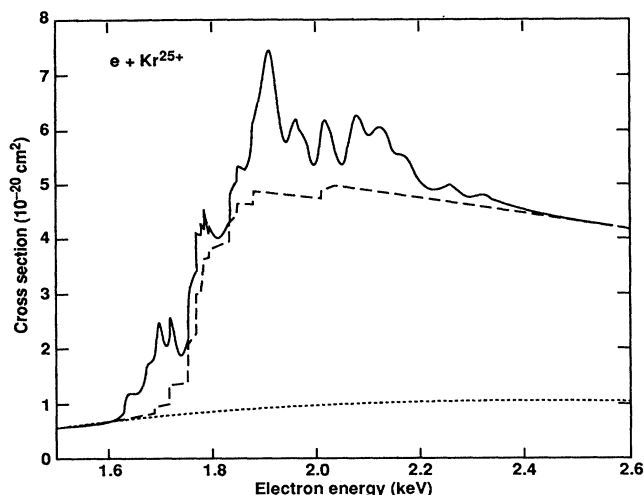


FIG. 6. Electron-impact ionization cross sections for Kr^{25+} . The symbols are the same as in Fig. 5.

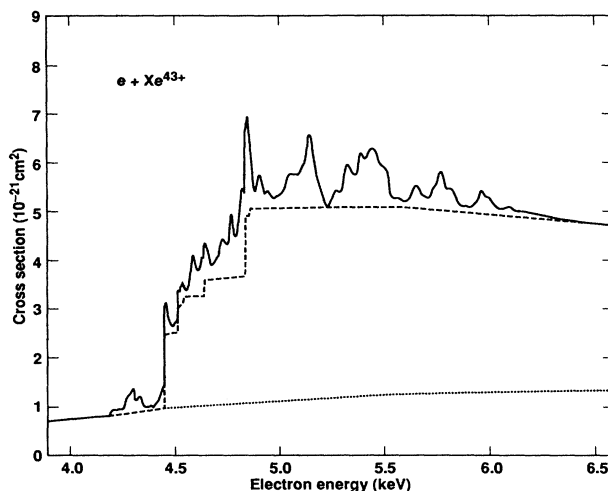


FIG. 7. Electron-impact ionization cross sections for Xe^{43+} . The symbols are the same as in Fig. 5.

like autoionizing states increases the Auger width and drastically reduces the effect of radiative damping for Kr^{24+} .

In earlier studies of Na-like ions, the effects of including radiative transitions (e.g., $n=3$ to $n=3$) in the calculation of EA cross sections were found to be very small for ions with $Z \leq 54$ [10]. The $\Delta n=0$ transitions are neglected in this work.

In Figs. 3 and 4, the computed REDA cross sections for Kr^{24+} and Kr^{25+} are shown. To facilitate comparison with planned experiments [15] on the electron-beam ion trap at LLNL, each REDA resonance has been convoluted with a Gaussian 16 eV in width. For incident electron energies $1.6 \leq E \leq 1.8$ keV, the cross sections are dominated by contributions from the $2p^5 3s 3nl'$ intermediate states for Kr^{25+} and by contributions from the $2p^5 3s^2 3dnl'$ state for Kr^{24+} . In the range $1.8 \leq E \leq 2.2$ keV the largest contributions for Kr^{25+} are from the $2p^5 3s 4nl'$ intermediate states, and the largest contributions for Kr^{24+} are from the $2p^5 3s^2 4nl'$ states.

The direct-ionization, excitation-autoionization, and total ionization cross sections including the REDA contributions for Kr^{24+} , Kr^{25+} , and Xe^{43+} are displayed in Figs. 5–7. As in the case of other highly charged Na-like ions [10] the EA process enhances the ionization cross section by a factor of 4 for Kr^{25+} . For Kr^{24+} , the contri-

bution from the indirect processes is about 2.5 times the direct-ionization cross section. The enhancement in Kr^{24+} is smaller than that in Kr^{25+} because the additional $3s$ electron doubles the direct-ionization cross section. Similar to the case of Fe^{15+} [9], the REDA process produces many strong resonances. At incident electron energies near 1.7 keV the REDA resonances enhance the ionization cross sections by a factor of 2 for Kr^{24+} and Kr^{25+} . For $1.9 \leq E \leq 2.2$ keV, the REDA process contributes between 10% and 30% of the total cross section. In Xe^{43+} the REDA process contributes as much as 25% to the total ionization cross section for $4.2 \leq E \leq 6$ keV.

In summary, we have calculated electron-impact ionization cross sections for Kr^{24+} , Kr^{25+} , and Xe^{43+} using relativistic distorted-wave and MCDF methods. We found that the indirect processes make far greater contributions to the ionization cross sections than the direct ionization in Mg-like Kr as well as in Na-like Kr and Xe. New precision experiments are needed to test these theoretical results.

ACKNOWLEDGMENTS

This work was performed under the auspices of the U.S. Department of Energy by Lawrence Livermore National Laboratory under Contract No. W-7405-ENG-48.

- [1] R. A. Falk *et al.*, Phys. Rev. Lett. **47**, 494 (1981).
- [2] K. T. LaGattuta and Y. Hahn, Phys. Rev. A **24**, 2273 (1981).
- [3] D. C. Griffin *et al.*, Phys. Rev. A **29**, 1729 (1984).
- [4] M. S. Pindzola and D. C. Griffin, Phys. Rev. A **36**, 2628 (1987).
- [5] M. H. Chen, Nucl. Instrum. Methods B **43**, 366 (1989).
- [6] N. R. Badnell, M. S. Pindzola, and D. C. Griffin, Phys. Rev. A **43**, 2250 (1991).
- [7] M. H. Chen and K. J. Reed, Phys. Rev. A **45**, 4525 (1992).
- [8] K. J. Reed and M. H. Chen, Phys. Rev. A **45**, 4519 (1992).

- [9] M. H. Chen, K. J. Reed, and D. L. Moores, Phys. Rev. Lett. **64**, 1350 (1990).
- [10] K. J. Reed, M. H. Chen, and D. L. Moores, Phys. Rev. A **41**, 550 (1990); **42**, 5315 (1990); **44**, 4336 (1991).
- [11] H. L. Zhang and D. H. Sampson, Phys. Rev. A **42**, 5387 (1990).
- [12] P. L. Hagelstein and R. K. Jung, At. Data Nucl. Data Tables **37**, 17 (1987).
- [13] M. H. Chen, Phys. Rev. A **31**, 1449 (1985).
- [14] I. P. Grant *et al.*, Comput. Phys. Commun. **21**, 207 (1980).
- [15] D. Schneider (private communication).